Observations from the One Year Electric Field Study-North Slope of Alaska (OYES-NSA)
field campaign, and their implications for observing the distribution of global electrified
cloud activity

cloud activity
Thomas Lavigne ¹ , Chuntao Liu ¹ , Joseph Hill ¹ and Eric Bruning ²
¹ Department of Physical and Environmental Sciences, Texas A&M University-Corpus Christ
² Department of Geosciences, Texas Tech University, Lubbock, TX
Journal of Atmospheric and Solar-Terrestrial Physics
November 2020
Keys words:
Electric field, Global electric circuit, thunderstorms, precipitation, aerosols
Corresponding author address: Thomas Lavigne, Department of Physical and Environmental Sciences, Texas A&M University at Corpus Christi, 6300 Ocean Dr., Corpus Christi, 78412-5858
Email: tlavigne@islander.tamucc.edu

Abstract

For over a century, the electric Potential Gradient (PG) of the atmosphere has been measured and studied. The local vertical electric field (E_z) is strongly influenced by the presence of lightning, electrified clouds, rainfall, aerosols, and many others. The One Year Electric Field Study-North Slope of Alaska (OYES-NSA) field campaign was established in the summer of 2017 to measure the vertical electric field at the ARM site in Barrow, Alaska alongside a wide array of supplementary instrumentation, including a Micro-Pulse Lidar and upward facing Ka-band radar. Two years of observations (072017-062019) have shown the possibility to quantify the local effects from aerosols and clouds observed by the Lidar and Radar on the measured Ez. Throughout the manuscript, the physics convention of negative downward fair-weather electric fields is used. Three cases (convective clouds, high concentration of near surface aerosols, and blowing snow) are used to demonstrate the localized effects on the measured Ez. Utilizing the relationships between Ez and backscatter/reflectivity, we have developed a methodology to distinguish samples with local influences. A fair-weather (FW) condition is determined to be associated with a low Lidar backscattering (less than 15 km⁻¹sr⁻¹), in the presence of no significant cloud activity (radar reflectivity less than -10dBZ). The samples satisfying these criteria are found with a 5-minute averaged standard deviation of less than 15V/m, and E_Z between -250V/m to -50V/m. Using only properties of the E_Z measurements allows for the simultaneous comparisons of FW at multiple sites, without the need for supplementary information of local weather conditions. Simultaneous E_Z measurements from 8 FW cases are shown between Barrow, AK and Corpus Christi, TX on the timescale of minutes to hours. Similar variation patterns in the FW Ez are shown at both sites, providing evidence of the global nature of the atmospheric electric system. Furthermore, the seasonal-diurnal variability of FW at multiple sites shows similar distributions of the PG.

1. Introduction

Several atmospheric electricity variables such as lightning, thunder days, and the electric field are useful in monitoring the changing climate [Williams, 1992; Reeve & Toumi, 1999; Rycroft et al., 2000; Williams, 2005; Lavigne et al., 2019; among others]. In 2016, lightning was added for the first time to the Global Climate Observing System's (GCOS) list of Essential Climate Variables (ECVs). [Global Climate Observing System, 2016; Aich et al., 2018]. However, the major shortcoming in utilizing the lightning parameter to monitor the changing nature of global storms, is the relatively short time period of global coverage of lightning flash data [Christian et al., 1999; Aich et al., 2018]. Only several decades of optical imagers onboard satellites, as well as ground-based Very Low Frequency (VLF) networks are available on even the quasi-global scale. While these data are very useful for understanding the variability of lightning and thunderstorms at the diurnal, seasonal, and even inter-annual scales, they are not sufficient in understanding the longer-term trends (if any) that are occurring in thunderstorm activity during the past century [Christian et al., 1999; Rodger et al., 2006; Blakeslee et al., 2014a]. An interesting alternative is to instead monitor a global system that is largely driven by global thunderstorm and electrified cloud activity, that has a much longer data record. The Global Electric Circuit (GEC) of the atmosphere is a vast Earth system of electrical currents that are present between the Earth's surface and Ionosphere [Rycroft et al., 2008]. Even during fairweather conditions, in the absence of significant clouds, aerosols, etc., a small current density of approximately 2 pA/m² is always present running from the Ionosphere in the upper atmosphere, down to the Earth's surface [Rycroft et al., 2000]. Dating back to the early 20th century, it was hypothesized that the temporal variability of this fair-weather electric field, was produced by the simultaneous temporal variability of the summation global thunderstorm activity [Wilson, 1909;

Wilson 1921]. Whipple, [1929], provided the first quantitative evidence of the link between thunderstorms and the fair-weather field by utilizing ship-borne vertical electric field data aboard the Carnegie cruise. The results indicated the maxima of both the GEC and thunder day area to occur at approximately 19 UTC, while the minima occurred at roughly 3 UTC. This diurnal cycle of the fair-weather electric field measured during this ground-breaking field work is now known as the classical Carnegie Curve [Harrison, 2013]. It remains the present-day view that the totality of thunderstorms around the globe at any given time, act as the main "battery" that continuously drives the GEC [Williams, 2009].

Throughout the next 90 years, many more details about the GEC have been revealed. With the addition of far greater amounts of electric field data measured around the globe, further details have been uncovered pertaining to the diurnal [Burns et al., 2005; Liu et al., 2010; Mach et al., 2011; Nicoll et al., 2019; among many others], seasonal [Adlerman & Williams, 1996; Liu et al., 2010; Burns et al. 2012; Blakeslee et al., 2014b; among many others], interannual [Burns et al., 2005; Williams & Mareev, 2014; Lavigne et al., 2017] and even decadal [Markson, 2007] variability of the GEC. In the past several decades, the addition of quasi-global radar measurements from space, as well as optical lightning imagers, have allowed for thunderstorms, and electrified precipitation systems to be analyzed in greater detail [Christian et al., 1999; Goodman et al., 2013]. The combination of the improvements in coverage of electric field measurements, as well as vast advancements in the global measurement of thunderstorm and cloud activity, has allowed for corroboration and extension of Wilson's and Whipple's findings.

The El Nino Southern Oscillation (ENSO) variability has also been observed in fair-weather electric field data [Hamid et al., 2001; Satori & Williams, 2009; Lavigne et al., 2017]. The regional increases and decreases in thunderstorm and electrified cloud occurrence on the

ENSO time scales has been noted to also be simultaneously observed in the fair-weather electric field measured in Vostok Station, Antarctica [Lavigne et al., 2017]. For example, during the Southern Hemispheric summer months, an increase in both precipitation from thunderstorm and electrified clouds, as well as flash count was observed by the Tropical Rainfall Measurement Mission (TRMM) satellite during the hours of 16-24 UTC in La Nina periods. South America, which is known to be convectively active during this time, also observes an increase in thunderstorm and electrified clouds during these La Nina periods [Williams and Stanfill, 2002; Liu et al., 2010, Lavigne et al., 2017]. This increase in both electrified precipitation features, as well as the GEC during this time period, indicates that indeed the regional enhancement/suppression of thunderstorms as a result of ENSO can simultaneously be observed in the variation of GEC electric fields as well. This type of finding provides further evidence that the GEC is directly tied to the variability of global/regional thunderstorm and electrified cloud activity on a scale of natural climate variability (approximately 2-7 years). This allows for the next logical question to be asked; whether or not the GEC can monitor the longer-term climate variability over the past 100-years?

For all the progress that has been made on understanding and modelling the GEC of the atmosphere, there are still many unknowns pertaining to the smaller-scale contributing input parameters. *Kalb et al.*, [2016] had some success at parameterizing storm conduction currents in the TRMM domain, and applying them to a global Earth model. However, the output models had a significantly smaller diurnal amplitude, and peaked approximately 4-6 hours before the Carnegie curve. This could imply that there are several other factors not included in the budget that play an important role in driving the GEC system. As a general rule, thunderstorms and electrified showerclouds (defined as precipitation systems that produce significant charge

separation but do not generate lightning) are the main driver of the GEC [Rycroft et al., 2007; Mach et al. 2009; Liu et al., 2010; Peterson et al. 2018]. However, it has been well established that many other physical processes contribute to the system. These include cosmic galactic rays, geomagnetic processes, energetic solar particles as well as many others [Tinsley, 2000; Siingh et al., 2007; Baumgaertner et al., 2013, among others]. In addition to these, many other localized processes are known to influence the local vertical electric field, such as aerosols, non-raining clouds, blowing dust and snow, fog, radon gas release, auroras, etc.

Several past studies have examined the influence of several of the above-mentioned localized influences on the measured vertical electric field. The typical magnitude of the physics convention fair-weather electric fields measured on the surface at sea level varies from approximately -100 to -200 V/m. It should be noted that throughout this manuscript, the physics convention of fair-weather electric fields will be used. Fair-weather electric fields will be represented as negative, and the potential gradient will be represented as positive values. Lucas et al., [2017] concluded using that during fog conditions, the Earth's electric field deviates from the background fair-weather electric field by roughly +150-200 V/m. The same study concluded that during an overcast day, the electric field varied by approximately -40 to -50 V/m from typical fair-weather values. This indicates that non-electrified clouds and fog contribute relatively weakly to the localized electric field. However, several studies have shown that blowing snow can cause a much larger influence on the electric field. Schmidt et al. [1999] concluded that surface electric field measurements during even a moderate blizzard can deviate the electric field on the order of +30,000 V/m. Model outputs conducted by Gordon and Taylor [2009] seem to corroborate this result, indicating that electric field magnitudes can exceed 25,000 V/m during surface blowing snow events. Chmielewski [2013] studied the influence of

blowing dust on the surface vertical electric field in West Texas. The study found that a typical blowing dust event causes a +4000 to +5000 V/m effect on the electric field. However, during intense events, the effect can be as a large as +15,000 V/m based on case studies.

At high latitudes, snow cover may slow the release of radon from the ground which changes the conductivity of the near-surface atmosphere. *Baumgaertner et al.*, [2013], found that direct natural radiation emitted from surface, as well as ground decay of radon gas, lead to approximately 10 ion pairs cm⁻³s⁻¹ over land between the latitudes of 60°N-60°S. In higher latitude regions where ground snow coverage is more prevalent, the rate was found to be reduced to half, creating a variation in the surface conductivity of up to 200% [*Baumgaertner et al.*, 2013].

Furthermore, in high-latitude regions, aurorae are present. These solar wind disturbances can have intense effects on localized electric field measurements in polar regions. A case study, conducted by *Olson* [1971], concluded that during an incident of visual aurora near the measurement site, the surface electric field was disturbed on the order of 1000 V/m for several hours. During this time period, the sky was clear with no visible clouds indicating that the significant jump in the surface electric field was due to the solar event. The study further indicated that there are two main types of aurorae events: 1) events that produce negative E_z for approximately 30 minutes and then return to fair-weather magnitudes, and 2) events that more significantly shift the E_z towards negative values, and last on the order of several hours [*Olson*, 1971]. More recent studies on aurora influence such as *Lucas et al.*, [2015], concluded that in arctic regions of the globe, the amplitude of magnetospheric perturbation can be as large as 50% of the GEC potentials, and can either constructively or destructively interfere. *Reddell et al.*, [2004], conducted a magnetospheric correction due to the cross-cap potential of the vertical

electric field. This diurnal correction was found to have the largest sinusoidal variability of +15 V/m at roughly 7 UTC and -25V/m at approximately 21 UTC during periods of high magnetic activity. This correction factor was found to be in good agreement with several other past studies at high latitudes [*Tinsley et al.*, 1998; *Corney et al.*, 2003].

To address the mystery of the localized inputs to the electric field, as well as to build upon the understanding and possible practical uses of the global aspect of the GEC, a field campaign has been created in the unique location of the North American Arctic. The One-Year Electric Field Study-North Slope of Alaska (OYES-NSA) field campaign was established in June of 2017 at the Department of Energy (DOE) Atmospheric Radiation Measurement (ARM) Northern Slope of Alaska (NSA) site. With the goal of understanding the contribution of the unique localized parameters in the region to the electric field, as well as to utilize the fair-weather electric field to monitor electrified cloud activity around the globe, this student-led field campaign was established in the northernmost town in the USA, Barrow, Alaska.

The North Slope of Alaska (NSA), provides a unique study site to monitor both local influences on the vertical electric field, as well as the fair-weather global component. The region observes unique Arctic cloud formations, which have shown at times to become significantly electrified. The North Slope of Alaska is an ideal location for measuring these electric field values, due to the stably stratified boundary layer that exists in the extremely cold temperatures [*Burns et al.*, 2005]. In addition to the unique nature of the site (i.e. blowing snow, Arctic clouds), the site is also very well instrumented. The location has a co-located Ka-band radar, a Micro-Pulse Lidar (MPL), as well as much other supplementary meteorological information.

The unique vertical separation of two electric field meters (one at 2 m and the other at 5 m), allows for the investigation of local space charge concentration in the region. *Marshall et al.*

[1999], studied the sunrise effect in the fair-weather electric field at Kennedy Space Center in Florida. Results from the study found that enhancement measured near sunrise was due to the upward mixing of the dense electrode layer very near the surface. The presence of two electric field mills separated by several meters can help determine if the conductivity changes above the electric field mills, or if local space charge is introduced such as in the cases that Marshall studied.

The site, which is one of the only electric field records in the Western Hemispheric Arctic, aims to shed light on the contribution of the unique local influences on the electric field budget, as well as to monitor the global component or GEC from the Arctic, in order to better understand the variability of global thunderstorms and electrified clouds at various timescales.

2. Data and Instrumentation

2.1 Study Location

The OYES-NSA field campaign instrumentation site is located on the grounds of the DOE ARM North Slope of Alaska site. The site is located at approximately 71.3°N and 156.6°W, near Barrow, Alaska, making it the northernmost electric field monitoring site in the United States. In addition to the main study site of the field campaign, a supplementary electric field observation is simultaneously monitored in the sub-tropical region of Corpus Christi, Texas. This site is located at 27.7°N and 97.3°W on the Texas A&M University-Corpus Christi campus. Figure 1b displays a map of the geographical location of both of the electric field meter sites separated by 6015 km.

2.2 Instrumentation

Figure 1a shows the main instrumentation setup at the Barrow, AK site. At this location, two Campbell Scientific (CS110) electric field mills are positioned at two different heights. The lower CS110 is set at approximately 2 m off the ground, while the higher field mill is oriented at approximately 5 m off the ground. This setup allows for a slight vertical profiling of the near-surface electric field, which could help understand the influence of blowing snow and other surface interactions. In addition to the two electric field meters, a RM Young Alpine anemometer is located near the lower electric field meter. The CS110 electric field mills are set up to sample at a rate of 1 Hz. It is important to note that the CS110s measure the vertical electric field in the orientation in which fair-weather fields (downward fields) appear negative.

The white building located in distance of the field meter setup in Figure 1a (approximately 100m away) houses the data retrieval computer, as well as supplementary instrumentation sources. On the top of this building, sits a vertical pointing Ka-band radar (KAZR), as well as a vertical profiling 532 nm Micro-Pulse Lidar (MPL), as well as many other instruments maintained at the DOE ARM site.

The Corpus Christi, TX site includes one CS110 that also samples at a rate of 1 Hz. This field meter is set at approximately a 2 m height. The location includes supplementary temperature, wind, relative humidity, solar irradiance from a weather station 10 m away from the CS110.

2.3 Calibration

In order to establish a ground surface measurement of the vertical electric field at the NSA and Corpus Christi sites, rigorous calibration was conducted. To remove the influence of the metal mounting poles, as well as other nearby instrumentation setups, a ground-level upward

facing measure of the vertical electric field was taken similtaneouly to the downward facing CS110s on the pole. The upward facing measurement was taken far away (greater than 3-times the distance of the height) from any metal or powerline influences, and provides the "true" undisturbed vertical electric field measure. The two operational CS110 instruments on the pole were then calibrated to match these values using a linear calibration multiplier and intercept [Chmielewski, 2013]. The simple calibration equation is as follows:

$$Ez_{ground} = a \bullet Ez_{pole} + b \tag{1}$$

Where Ez_{ground} is the ground flush electric field meter measurement (V/m), Ez_{pole} is the raw electric field measurement on metal pole (V/m); a and b are slope and intercept constants after the linear regression.

Figure 2 shows the calibration process. As the metal mounting setup causes the vertical electric field lines to bend toward the pole, calibration is needed to correct for this effect. As shown in Figure 2a and Figure 2c, the calibration factor for the 5m CS110 is a multiplier of 0.823 and intercept of -54.9, while the factor for the 2m CS110 was determined to be a multiplier of 3.121 and an intercept of 16.69. With the inclusion of these calibration factors, the metal-mounted CS110s match the undisturbed ground-flush E_z measurements at a near 1-1 relationship, indicating an "absolute" measure of the Ez_{ground} . This ground-flush calibration process was repeated at the Corpus Christi site, resulting in a calibration factor of 1.747 and the intercept of 42.55. It should be noted that in November of 2018, a CS110 instrument swap took place due to maintenance of the preexisting instrument. Rigorous testing concluded that an instrument swap resulted in an absolute electric field discrepancy of less than 10 V/m, which is well within the margin of error of the CS110 of +/- 5% +8 V/m.

2.4 supplementary data

One of the advantages of monitoring the electric field at the North Slope of Alaska DOE ARM site, is the availability of supplementary instrumentation on site. The site is home to multiple radars, a Micro Pulse Lidar (MPL), as well as numerous other meteorological measuring equipment.

The Ka-Band radar, also known as the KAZR, is an upward pointing Doppler radar that operates at a frequency of approximately 35 GHz. The three main return measurements are, reflectivity, vertical velocity and spectral width. The sample rate is 30 seconds and measures in a vertical range of approximately 30 m to 20 km. The MPL lidar is an upward pointing optical remote sensing instrument, that is used to detect aerosols as well as cloud altitude. The MPL operates at a wavelength of 532 nm. The MPL samples every 30 seconds with vertical resolution of 15 m, with a maximum height of approximately 20 km. For the purpose of this study, 5-minute maximum column backscattering coefficient are used, which denotes the maximum backscatter signal observed by the MPL anywhere in the vertical column during the 5-minute period of time. Both KAZR and MPL lie approximately 100 m (near the background building in Figure 1a) from the electric field measurement site.

To determine blowing snow, fog, as well as haze days in Barrow, Alaska during the operating period of the field campaign, the National Climatic Data Center (NCDC) Monthly Climate Data F6 product is used. This dataset includes the daily maximum and minimum temperatures, dew point temperature, precipitation, snow depth, wind speed and direction, as well as a weather flag. The weather flag indicates a binary occurrence of events such as fog, thunder, ice pellets, hail, freezing rain, dust, haze, smoke and blowing snow. The location of the data collection is in the town of Barrow, Alaska (71.17 N, 156.47 W.)

3. Results

3.1 Examples of influences on the electric field by various factors

In order to better understand how the supplementary data can be used to interpret deviations observed in the vertical electric field measurements, four example cases are shown under different and unique environmental conditions. The four following cases all occur in Barrow, Alaska and are shown with the Ez_{ground} from the calibrated 5m CS110 measurements.

3.1.1 Significantly Charged Precipitation Event

Figure 3 shows an event in Barrow, AK in which a significant precipitation event crossed overhead of the instrumentation. The case occurred during the warm season on July 3, 2018. At approximately 23:25 UTC, a leading anvil edge began to pass above the field meter at an altitude of approximately 2.5 km (Figure 3a). This cloud introduced a strong negative field (Figure 3b) on the order of -5000 V/m. During this time period, no precipitation appears to be present on the ground as evidenced by Figure 3a and Figure 3c displaying no significant radar reflectivity below 3km, as well as no lidar backscattering signature near the surface. At approximately 23:30, larger reflectivity appears overhead at the field meter and at lower altitude. This more convective-like signature (>30 dBZ) begins to gradually drive the electric field strongly positive, reaching a maximum of roughly +12,000 V/m. It appears that two separate raining cells are present. In between, a radar bright band and lower reflectivity at the surface suggests a short period of stratiform-like non-raining cloud, associated with a negative dip in the electric field at approximately 23:35 UTC.

This relatively highly-electrified case (for the Arctic) indicates that the Ka-band radar can be very useful in determining large variation and swings in the electric field. Clouds with reflectivity greater than 20 dBZ show strong qualitative correlation to the electric field variability

and magnitude. Furthermore, the Ka-Radar shows the ability to distinguish different cloud-regions of the precipitation events such as the leading anvil, convective, raining, stratiform, etc. Strongly electrified cases also show that the MPL is almost instantly fully attenuated upon the presence of the strong precipitation feature (Figure 3c). Other than the possible use of determining precipitation at the near-surface, the MPL can also be useful in determining that the surface air was relatively clean for this case.

3.1.2 Aerosol/Lidar Dominant Event

Figure 4 shows an event that occurred on August 12, 2017. The case exhibits a very stable cloud that occurs from approximately 3 km up to 8 km (Figure 4a) throughout the entire 7-hour case. Despite the relatively stable and unchanging Ka-radar reflectivity, Figure 4b shows that strong short-lived jumps in the vertical electric field are present throughout the case, on the order of +400 to +700V/m. This variability is simultaneously observed very clearly in the MPL backscattering signature in Figure 4c. Very clear backscattering on the order of 250-400 km⁻¹Sr⁻¹ in the lower 200-300m of the atmosphere is observed during the time of the electric field spikes. Figure 4c shows that the particles causing the strongest backscatter occurs very near to the surface. This indicates that the spikes observed in the electric field are caused by aerosols or cloud very near to the surface that are difficult to observe with the Ka-radar. Examples of this type of signature could be dust, salts, fog, etc. very near to the surface. Due to the case taking place in the warm season, this is not consistent with a blowing snow type event.

This type of case is frequent in the NSA region throughout the year, with short lived spikes in the electric field observed nearly every day. The MPL backscatter is shown to be very useful in determining these time periods, with a high visual correlation between the short-term electric field variability and backscattering in the lower 0.5 km of the atmosphere. The variability

of the electric field in cases such as these is not clearly observed in the Ka-reflectivity (figure 4a). This indicates that these low reflectivity stratus clouds are not the driving cause of this E_z variability shown in Figure 4. When the near surface aerosol information is also simultaneously observed, it is clear that the E_z variability is well correlated to the short-term variations of high backscattering from the near surface. This illustrates the importance of being able to monitor the cloud as well as surface aerosols when understanding the variability of the E_z .

3.1.3 Blowing Snow Event

Figure 5 shows an event that occurred on November 9, 2018. This event occurred during the cold season in the NSA. Based on the NCDC F6 product, surface observations, the temperature varied from -13.3 to -6.7°C and also indicates a snow pack was present on the ground with a depth of 7 inches. The initial period of the case (8-11 UTC) shows very little if any cloud activity according to the Ka-reflectivity (figure 5a). Likely due to blowing snow covering the instrument, the MPL did not collect any useful information for this case. During this time period, Figure 5b shows that a variability of both the 2m electric field meter (red) and the 5m electric field meter (blue) of approximately 100V/m is present in the vertical electric field, with sharp jumps present. This variability correlates to both the U-vector wind speed with a correlation coefficient of 0.45 (Figure 5c), as well as qualitatively to the total wind speed (Figure 5d). This indicates that during this case, particles are blown aloft in the wind, and simultaneously influence the vertical electric field due to the conductivity change. During periods with wind speeds above 2 m/s, the electric field becomes less negative (-25 to -50 V/m). Based on the study by *Schmidt* [1982], an approximate 3-5 m/s wind speed is required to start larger-scale blowing snow transport. However, based on figures 5c and 7, it appears that very small ice particles (less

than blowing snow requirements) begin to be thrown aloft at 2m/s wind speed and start to influence the conductivity of the air. This is possibly the cause of the relatively larger difference observed between the 2 m CS110 and the 5 m CS110 when the wind speed becomes greater than approximately 2 m/s (Figure 5b). This is observed because the two electric field mills are no longer encountering the same environment, with the lower elevated CS110 theoretically surrounded by a larger number of tiny particles due to the wind. When the winds return to approximately 1 m/s, both the 5 m and 2 m electric field mills sharply recover back to normal fair-weather values for this time of year of approximately -150 to -200 V/m.

Blowing snow events are very common in the NSA, which observes nearly year-round, except a few months in summer, snow coverage as well as high winds throughout the year. This case emphasizes the extremely common very low magnitude blowing snow events (50 to several hundred V/m) that are nearly always present in the winter months. During blizzard conditions, much more obvious deviations on the electric field are present. It is very important especially when considering fair-weather to be able to identify these very weak but significant deviations in the E_z caused by snow particles aloft.

3.1.4 Aerosol Influence Event

Figure 6 shows an event that occurred on July 1, 2017. Figure 6a displays that almost no precipitation activity was present during the entire case, with several small clouds of less than - 10 dBZ occasionally present around 4-5 and 9-10 km. However, the vertical electric field observed significant variability throughout most of the day on the order of magnitude of several hundred V/m. The variability observed in the electric field (Figure 6b) corresponds to the simultaneous presence of MPL backscattering (Figure 6c). During periods of relatively intense backscattering (>100 km⁻¹Sr⁻¹), the standard deviation of the E_z increases, fluctuating several

hundred V/m in the timespan of less than an hour. However, there is a time period where there are no significant clouds (>-10dBZ), as well as virtually no MPL backscattering between the hours of approximately 3-9 UTC. During this time period of no observed electrified clouds or aerosols, a very stable vertical electric field is present at approximately -150 to -200 V/m, which is consistent with the fair-weather range. This period of time can be presumed to be measuring the fair-weather vertical electric field, representing the true global component of the E_z, known as the GEC.

It should be noted that even non-electrified clouds, potentially such as the low reflectivity clouds observed in Figure 6 between 2-8 UTC at an altitude of approximately 9-10 km, can still influence the current density of the fair-weather return current [Baumgaertner et al.,2014]. Clouds such as these in the fair-weather region of the GEC were found to increase global resistance by up to 73% of the cloud free atmospheric resistance [Baumgaertner et al.,2014]. Furthermore, a single cirrus cloud similar to the cloud observed in Figure 6, was found to create a strong reduction of the average current density from approximately 2.5 pAm⁻² to 0.6pAm⁻² [Baumgaertner et al.,2014]. The influence of these non-electrified clouds to the determination of fair-weather in the NSA region should be addressed further in the future.

This case study result indicates the possibility of quantitatively utilizing radar observed cloud and Lidar indicated aerosol data to be able to determine these fair-weather periods with more precision. This is extremely important for the NSA site where these periods of fair-weather are not common. Being able to piece together shorter periods (minutes to hours) of fair-weather into a composite is crucial at NSA to understand the variability of the GEC measured at the site.

3.2 Wind influence of the Vertical Electric Field

One objective of the OYES-NSA field campaign is to utilize the unique location of Barrow, Alaska to better understand how wind-blown particles can influence the electric field measurements. The location has the advantage of the presence of snow on the ground for much of the year, as well as proximity to the Arctic Ocean (about 2 km to the coast). This allows for the opportunity to study situations of blowing snow, fog, sea salt, dust, among others. Even under conditions with no clouds present, this region observes days with large Ez deviations from fair-weather values. Figure 7 shows the difference in the Ez measurements between the two CS110s each at a different height versus the wind speed for two months, one in the cold season (Figure 7a-b) and the other in the warm season (Figure 7c). In Figure 7a, the color fill indicates blowing snow days in Barrow, AK as determined by the National Climatic Data Center (NCDC) monthly climate data F6 product for the month of January 2018. The contours indicate hazy days determined by the NCDC F6 product. Figure 7a shows that a threshold of approximately 2 m/s is needed to start to significantly deviate the recordings from the two instruments from one another, which is supporting the blowing snow scenarios. With wind speeds of approximately 2-5 m/s, the 5m electric field meter tends to record a significantly lower E_z reading of up to -2000 V/m. The presence of both the color fill, as well as contours, indicate that this influence from wind could either be due to blowing snow or haze. However, when the wind speed reaches 8 m/s and above, only blowing snow days are present, and the 5 m CS110 tends to record larger Ez values than the 2 m CS110, up to 1000 V/m.

Figure 7b compares blowing snow days vs. clear days in Barrow Alaska as determined by the NCDC F6 data. A clear day is defined as having no significant weather events as defined by the NCDC (i.e. fog, thunder, ice pellets, freezing rain, dust, smoke, haze, blowing snow, etc.)

The contours show that on clear days in the cold season, a much smaller deviation between the

5m and 2m CS110 is present when the wind speed is higher than 2 m/s. The vast majority of the measurements occur within 100 V/m of each other, with most much closer than that. It is also important to note that no clear days were recorded with wind speeds above 6 m/s during the month.

Figure 7c exhibits the difference between the 5-m and 2-m electric field mills in a warm month of August 2018. There is much less deviation between the top and bottom CS110s as a function of wind speed in summer. This is likely due to the fact that no ground snow is present in August in this area. Figure 7c shows that a few cases above 6 m/s, tend to deviate the two CS110s from one another (up to 2000 V/m), These periods of time were determined to be significant raining events as shown in Figure 3, and not related to the surface wind environment.

It should also be pointed out that although this work focuses on the blowing snow effect on the difference between the measured E_z at the 5 m and 2 m electric field mills, some of the difference could be due to surface radon release, which could also influence the conductivity of the air. The difference between the 5 m and 2 m electric field mills in the winter months, corroborates this as radon release can be suppressed by the presence of ground-based snow [Baumgaertner et al., 2014]. This creates an electrode layer near the surface could potentially produce a vertical gradient of E_z [Marshall et al., 1999]. Further investigation is needed in the future to quantify the influence of radon release on the vertical electric field at the NSA site.

3.3 Determination of Fair-Weather

3.3.1 Lidar Determination of Fair-Weather

One great advantage of locating the OYES-NSA field campaign at the DOE ARM site, is the plethora of supplemental instrumentation available. As shown in the above cases (Figures 36), the MPL lidar is very useful in determining periods of high amounts of aerosols, rain occurrence, low-level cloud activity, etc. This indicates the possible usefulness of this instrument in helping to select periods of fair-weather electric fields. Figure 8 exhibits averaged E_z values versus the maximum column MPL backscatter coefficient within 5-minute intervals observed on June 6, 2018. A clear separation is found between the samples with a backscattering of less than 250 km⁻¹sr⁻¹ and those above. MPL periods with backscattering greater than 250 km⁻¹sr⁻¹ show a large spread in corresponding E_z values. However, when the maximum MPL backscattering coefficient falls below 250 km⁻¹sr⁻¹, a clear grouping of E_z measurements is present in the range of -50 to -125 V/m. This range of values is within the known fair-weather range for this time of year.

Figure 8b shows the 5-minute binned maximum column MPL backscatter coefficient versus the standard deviation of each 5-minute period of the vertical electric field (E_z). Again, with a backscattering of less than 250 km⁻¹sr⁻¹, a clear separation of standard deviation values is present. When aerosol or clouds are present with a backscattering coefficient greater than 250 km⁻¹sr⁻¹, E_z values tend to have larger variations. With the presence of very little backscattering a grouping of 5-minute averaged standard deviation values of less than 20 V/m is present, indicating a relative stable electric field.

3.3.2 Case Study Composite of Absolute Value and Standard Deviation Determination of Fair-Weather

Figure 9 shows the relationship between the MPL backscattering and the E_Z in a 10-case composite. All cases are selected in 2018, and include: April 9th, April 10th, May 3rd, May 10th,

May 30th, August 22nd, September 9th, October 14th, October 15th, and December 18th. All cases have relatively long (>2 hour) periods of low Lidar backscattering (<250 km⁻¹sr⁻¹) which is extremely rare for the NSA region. Figure 9a shows a scatterplot of the 5-minuted averaged electric field (E_z) versus the simultaneous 5-minute standard deviation of the electric field (E_z). Green markers represent 5-minute periods of time determined to be fair-weather by the MPL lidar, with maximum reflectance values of less than 150 km⁻¹sr⁻¹ in the vertical column. Red markers indicate 5-minute periods of time determined to be non-fair-weather by the MPL lidar with maximum reflectance values of greater than 150 km⁻¹sr⁻¹ in the vertical column. Figure 9b zooms in on the lower magnitude electric field values. A clear separation between MPL determined fair-weather and non-fair-weather is present in the composite, with 5- minute averaged fair-weather occurring in the vertical electric field range of -50 to -350 V/m with simultaneous standard deviations of less than approximately 25 V/m.

Utilizing this Lidar assisted composite, a simple definition of fair-weather can be created using only the E_z measurements themselves, requiring no use of supplemental instruments such as radars or lidars. This definition is determined to be a 5-minute averaged absolute measurement of the electric field in the range of -50 V/m to -350 V/m, with a simultaneous standard deviation of less than 25 V/m. This includes only E_z measurements in the known fair-weather range that are very stable. This allows for the simultaneous comparison to other electric field measurement sites without lidar observations. This stringent definition includes only the strictest fair-weather and most stable values to be included, in order to assure as many local influences are removed as possible.

Nicoll et al., [2019], introduces the Global Coordination of Atmospheric Electricity

Measurements (GloCAEM) dataset, which includes 17 locations worldwide. In the case of this

dataset, meteorological data is only available at some of the measurement sites, making "True" fair-weather conditions difficult to explicitly identify [Nicoll et al., 2019]. This dataset utilizes "non-disturbed" electric field values defined as the inner 80% of the electric field distribution. Both the method outlined above in this study, as well as the GloCAEM method attempt to remove outliers of the electric field caused by many events such as precipitation, lightning, aerosols, blowing snow, etc. However, results of this study show that there are indeed instances of electric field measurements inside the 80% normal distribution that have significantly large standard deviations that could be still influenced by local disturbances.

3.4 Variability of Fair-Weather at Several Timescales at Multiple Sites

3.4.1 Diurnal Variability

Figure 10 applies the fair-weather definition developed in Figures 8 and 9, now represented as the potential gradient, to two separate sites (Barrow, AK and Corpus Christi, TX) for the entire year of 2018. Figure 10a shows the comparison in two separate months, May (red) in the warm season, and October (blue) in the cold season. The solid lines represent the Barrow, AK diurnal variability, and the dashed lines represent the Corpus Christi, TX diurnal cycle. All data is binned hourly. A very similar qualitative agreement is observed between the simultaneous diurnal variability recorded at the two sites. Corpus Christi, which has far more fair-weather samples, appears to be much smoother, but in general both sites follow a very analogous diurnal maxima and minima in the observed fair-weather potential gradient. Both sites recorded absolute electric field measurements in the range reported by the Carnegie cruises. Due to slight differences in site location, calibration, instrumentation etc., an offset of approximately 10-30 V/m is present between the two sites, with Corpus Christi recording consistently larger potential

gradient values. However, this difference falls within the standard measurement error range of the CS110 instrument (\pm +8 V/m).

Several other factors including time periods of snow coverage in Barrow, and nearly never freezing land in Corpus Christi, could lead to differences in the measured E_z, due to conductivity differences caused by the different rate of radon gas release [*Baumgaertner et al.*, 2013]. In addition, non-electrified clouds at both measurement locations could have different local effects on the electric fields, which have been shown to significantly influence the current density in the past [*Baumgaertner et al.*, 2014]. Another potential cause of observed deviation in the E_z between the Corpus Christi, TX and Barrow, AK sites is aurora events. Magnetospheric perturbation is known to significantly affect the high latitude region of Barrow (71.3°N), and could cause differences in the measured fair-weather E_z values, when compared to the subtropical Corpus Christi (27.7°N) location. A more detailed analysis of this effect is needed in the future.

It should be pointed out that the typical measurement recorded at the Corpus Christi site during fair-weather is between 0 V/m and -300 V/m, with the majority of measurements recorded between -100 V/m and -200 V/m. Applying the fair-weather definition determined in Figures 8 and 9, includes these values, and insures that only the most stringent fair-weather conditions are included from Corpus Christi, which has more frequent fair-weather time periods than Barrow.

Figure 10b shows the yearly averaged fair-weather diurnal cycle for the entire year of 2018. All three of the typical convective chimney regions are displayed in both of the diurnal curves; 7-10 UTC from the Maritime Continent, 12-15 from Africa, and 18-22 from the Americas. Both sites, which are separated by over 6,000 km, observe a similar diurnal pattern.

This indicates the truly global nature of the system when small periods of fair-weather are composited together. Furthermore, both sites follow a very similar diurnal pattern to the Carnegie Curve, which is the known standard for the diurnal variability of the GEC on UTC time, giving further support to the findings [Whipple, 1929].

3.4.2 Minute-to-Hour Fair-Weather Variability

In order to determine how fine of detail the GEC can be observed in the simultaneous fair-weather signature in Barrow and Corpus Christi, Figure 11 shows examples of fair-weather E_z time series on the order of minutes to several hours at both sites. All panels were again averaged to 5-minute bins. As in Figure 10, in all 4 cases, a similar inter-time-step variability can be observed in the time series at two sites. Differences of up to approximately 60V/m are present between the two sites, which could be due to slight differences in calibration, instrumentation or location. Further studies are required to explain this difference in more detail. However, for the purpose of this study, the pattern is of more importance when observing the variability of the GEC. Observing very similar time series on this fine temporal resolution in the strictly defined fair-weather values, indicates even further the global nature of the system. If this is true, the variability of global storm occurrence that drives the GEC can be monitored real-time on the scale of minutes to hours, instead of longer time scale monthly and yearly composites as first noted by *Markson* [1986]. More data is ultimately needed in order to verify this claim in the future.

3.5.2 Joint Diurnal Seasonal Variability

Much of the past work in comparing the GEC to thunderstorms and global electrified cloud parameters have been conducted utilizing electric field measurements taken in the Southern Ocean [Whipple, 1929] or Antarctica [Burns et al. 2005; Burns et al., 2012; Lavigne et al., 2017]. Another goal of the OYES-NSA field campaign is to establish a long-running time series of electric field measurements in the Arctic. Figure 12 compares the joint diurnal and seasonal comparison of the mathematically selected fair weather from the two poles. The data from Barrow was taken in 2018 and the data in Vostok Station, Antarctica was collected from 1998-2004 as well as 2007-2011. [Burns et al., 2005; Burns et al., 2007; Burns et al., 2012] Although a similar spatial pattern at both sites is observed such as the phase, there are also some significant differences. The variation amplitude is larger at the Barrow site, especially in the UTC hours of 15-22 from February to October. This amplitude difference could possibly be explained by the far fewer fair-weather samples in the Arctic. This points to the increasing need to continue sampling this valuable measurement in the Arctic. A long-term comparison between the poles could help to uncover more detail about what drives the system and how better to model it.

4. Discussion/Summary

4.1 Importance of supplementary data

The use of the DOE ARM supplementary site instruments such as the Ka-band radar and the MPL lidar, allows for the better understanding of how cloud, aerosols, blowing snow and fair-weather conditions appear in the electric field record on a case-by case basis.

• There is a strong response from the electric field to the presence of different types of clouds indicated by the radar reflectivity from the KAZR (Figure 3). Analyses of many

other electrified cloud cases in Barrow, AK as well as Corpus Christi, TX, confirm that leading anvils and stratiform regions can swing the electric field more negative on the order of several thousand V/m, as noted previously in *MacGorman & Rust* [1998]. Convective centers of the strongly electrified precipitation events have the opposite effect, driving the electric field highly positive. This magnitude varies, but is typically larger than the anvils and stratiform regions, with electric fields in the tens of kV/m observed.

- It is clear that the MPL observations help to link the relatively smaller-scale deviations in the measured E_z to small aerosol particles near to the surface (bottom 0.5 km), and not from electrified clouds or falling precipitation (Figure 4).
- The two vertically separated CS110s are able to detect the wind influence on the vertical electric field. The differences between 5-m and 2-m electric field mills is greater in the cold season (October-May) than the warm season (June-September). This is likely due to the presence of snow and ice/snow on the ground, which is easily sent aloft in even relatively low wind conditions (2 m/s). The particles blown in the air under 2-5 m/s wind tend to cause hazy conditions, as also noted by the local ground station. However, when wind increases to above 8 m/s in the cold season, it no longer creates these hazy conditions, and is more likely to cause blowing snow events, and deviates the two instruments from -1000 to +1000 V/m apart from each other.

4.2 Fair-Weather Analysis

Utilizing the backscattering signal from the MPL, a clear separation of electric field values and standard deviations is present in Figure 8. During periods of low column reflectance

of approximately less than 200-250 km⁻¹sr⁻¹, a grouping of very stable electric field measurements in the known range of fair-weather is clearly observed. This is corroborated by the case study shown in Figure 5, observing a very stable electric field of approximately -175V/m to -200 V/m during a period of virtually no surface backscattering or cloud activity. Although a 10-case composite is not ideal in determining the standard for a fair-weather definition, it provides a simple way of separating non-stable electric field periods (large standard deviations), as well as values that are known to fall outside the typical fair-weather range. Using this definition, similar patterns are found in the fair-weather fields on the time scales of yearly, monthly, minute to hourly averaged diurnal variability. These results corroborate past research stating the global nature of the system, at more refined timescales than previously explored. The consistent offset between the Corpus Christi, TX and Barrow, AK sites, with Barrow being consistently more negative but following the very similar temporal pattern, gives further support that both sites are encountering a very similar global contribution of electrified clouds and thunderstorms with slightly different calibrations.

4.3 Implications for Global Electrified Cloud Monitoring

With the temporal consistency between the fair-weather electric fields at multiple sites, it allows for the next logical step to verify if this variability is indeed driven by instantaneous electrified clouds and thunderstorms around the globe. Past work has verified that using longer term composites (multiple years), electrified precipitation feature parameters such as thunderstorm rainfall, flash rate, and volume 30 dBZ in the mixed phase region correlate very well on the time scales of diurnal, seasonal and interannual to the measured fair-weather electric field [*Liu et al.*, 2010; *Lavigne et al.*, 2017]. With this connection, it seems plausible to start to

look at the connection between the ground-based fair-weather electric field variability and the variability of global storms as well as other fine scale measurements at much smaller time scales. With the results shown in Figure 11, it seems plausible that the GEC can be detected simultaneously at multiple sites both encountering fair-weather without the need for averaging many smaller time periods together, as is the case in most classical diurnal depictions of the GEC. This, alongside improvements in satellite monitoring of precipitation such as the Integrated Multi-satellite Retrievals (IMERG), with near real-time global precipitation, allows for the possibility of understanding to what ability and at which timescales the GEC can monitor global electrified precipitation systems that act as its battery.

In addition to the valuable GEC measurements at the NSA site as well as other sites around the globe to monitor the contribution of electrified clouds and thunderstorms, the local electric field measurements in the Arctic may also allow for the unique opportunity to observe the effects of warming temperatures on the electrification of clouds and precipitation events in the region. A recent study observed that air temperatures in the Arctic have increased 2.7° C (4.9° F) over the past five decades [Box et al., 2019]. This rapid warming has likely influenced the types of clouds and precipitation systems in the region. During the first two full summer seasons (2018 & 2019) of the OYESNSA field campaign, the region has observed more than 10-events each year with at least +2,000 V/m electric fields, which are considered to be from electrically active clouds. A longer-term measurement of the electric field is needed to better understand the regions response to such rapid warming. With electrified shower clouds thought to precede thunderstorm activity, the preliminary results show that the region could observe significantly more electrified clouds if the current trends continue.

Acknowledgement

This study was supported by NSF-1519006. Thanks to the support of DOE ARM program allowing the setup of the instruments at NSA site. Thanks to Walter, Jimmy, Josh, Ross among many others for the support and maintenance of instruments at the NSA site. All NSA CS110 data are available at DOE ARM Site at:

https://adc.arm.gov/discovery/#/results/iopShortName::nsa2017oyesnsa as well as at Texas A&M Corpus Christi website: http://atmos.tamucc.edu/oyesnsa/data/

References

- Adlerman, E. J., & Williams, E. R. (1996). Seasonal variation of the global electrical circuit. *Journal of Geophysical Research: Atmospheres*, 101(D23), 29679-29688.
- Aich, V., Holzworth, R., Goodman, S. J., Kuleshov, Y., Price, C., & Williams, E. (2018). Lightning: A new essential climate variable. *Eos*, **99**. https://doi.org/10.1029/2018EO104583
- G. Baumgaertner, A. J., Thayer, J. P., Neely III, R. R., & Lucas, G. (2013). Toward a comprehensive global electric circuit model: Atmospheric conductivity and its variability in CESM1 (WACCM) model simulations. *Journal of Geophysical Research: Atmospheres*, 118(16), 9221-9232.
- Baumgaertner, A. J. G., Lucas, G. M., Thayer, J. P., & Mallios, S. A. (2014). On the role of clouds in the fair weather part of the global electric circuit. *Atmospheric Chemistry & Physics*, *14*(16).
- Blakeslee, R. J., Christian, H. J., Stewart, M. F., Mach, D. M., Bateman, M., Walker, T. D., ... & Colley, E. C. (2014a). Lightning Imaging Sensor (LIS) for the International Space Station (ISS): mission description and science goals.
- Blakeslee, R. J., Mach, D. M., Bateman, M. G., & Bailey, J. C. (2014b). Seasonal variations in the lightning diurnal cycle and implications for the global electric circuit. *Atmospheric research*, *135*, 228-243.
- Burns, G. B., Frank-Kamenetsky, A. V., Troshichev, O. A., Bering, E. A., & Reddell, B. D. (2005). Interannual consistency of bi-monthly differences in diurnal variations of the ground-level, vertical electric field. *Journal of Geophysical Research: Atmospheres*, *110*(D10).
- Burns, G. B., Tinsley, B. A., Frank-Kamenetsky, A. V., & Bering, E. A. (2007). Interplanetary magnetic field and atmospheric electric circuit influences on ground-level pressure at Vostok. *Journal of Geophysical Research: Atmospheres*, 112(D4).
- Burns, G. B., Tinsley, B. A., Frank-Kamenetsky, A. V., Troshichev, O. A., French, W. J. R., & Klekociuk, A. R. (2012). Monthly diurnal global atmospheric circuit estimates derived from Vostok electric field measurements adjusted for local meteorological and solar wind influences. *Journal of the atmospheric sciences*, 69(6), 2061-2082.
- Chmielewski, V. C. (2013). *Variations of the vertical electric field and wind speed on days with airborne dust in Lubbock, Texas* (Doctoral dissertation).
- Christian, H., Blakeslee, R., Goodman, S., Mach, D., Stewart, M., Buechler, D., ... & Bocippio, D. J. (1999, June). The lightning imaging sensor. In *NASA conference publication* (pp. 746-749). NASA.
- Corney, R. C., G. B. Burns, K. Michael, A. V. Frank-Kamenetsky, O. A. Troshichev, E. A. Bering, V. O. Papitashvili, A. M. Breed, and M. L. Duldig (2003), The influence of polar-cap convection on the geoelectric field at Vostok, Antarctica, J. Atmos. Sol. Terr. Phys., 65(3), 345-354, doi:10.1016/S1364-6826(02)00225-0

- Goodman, S. J., Blakeslee, R. J., Koshak, W. J., Mach, D., Bailey, J., Buechler, D., ... & Stano, G. (2013). The GOES-R geostationary lightning mapper (GLM). *Atmospheric research*, *125*, 34-49.
- Gordon, M., & Taylor, P. A. (2009). The electric field during blowing snow events. *Boundary-layer meteorology*, 130(1), 97-115.
- Hamid, E. Y., Kawasaki, Z. I., & Mardiana, R. (2001). Impact of the 1997–98 El Niño event on lightning activity over Indonesia. *Geophysical research letters*, 28(1), 147-150.
- Harrison, R. G. (2013). The carnegie curve. Surveys in Geophysics, 34(2), 209-232.
- Lavigne, T., Liu, C., Deierling, W., & Mach, D. (2017). Relationship between the global electric circuit and electrified cloud parameters at diurnal, seasonal, and interannual timescales. *Journal of Geophysical Research: Atmospheres*, 122(16), 8525-8542.
- Lavigne, T., Liu, C., & Liu, N. (2019). How Does the Trend in Thunder Days Relate to the Variation of Lightning Flash Density?. *Journal of Geophysical Research: Atmospheres*, 124(9), 4955-4974.
- Liu, C., Williams, E. R., Zipser, E. J., & Burns, G. (2010). Diurnal variations of global thunderstorms and electrified shower clouds and their contribution to the global electrical circuit. *Journal of the atmospheric sciences*, 67(2), 309-323.
- Lucas, G. M., Baumgaertner, A. J. G., & Thayer, J. P. (2015). A global electric circuit model within a community climate model. *Journal of Geophysical Research: Atmospheres*, 120(23), 12-054.
- Lucas, G. M. (2017). Investigating the physical mechanisms that impact electric fields in the atmosphere.
- MacGorman, D. R., MacGorman, R., Rust, W. D., & Rust, W. D. (1998). *The electrical nature of storms*. Oxford University Press on Demand.
- Mach, D. M., R. J. Blakeslee, M. G. Bateman, and J. C. Bailey, (2009). Electric fields, conductivity, and estimated currents from aircraft overflights of electrified clouds. *J. Geophys. Res.*, **114**, D10204, https://doi.org/10.1029/2008JD011495.
- Mach, D. M., Blakeslee, R. J., Bateman, M. G., & Bailey, J. C. (2010). Comparisons of total currents based on storm location, polarity, and flash rates derived from high-altitude aircraft overflights. *Journal of Geophysical Research: Atmospheres*, 115(D3).
- Mach, D. M., Blakeslee, R. J., & Bateman, M. G. (2011). Global electric circuit implications of combined aircraft storm electric current measurements and satellite-based diurnal lightning statistics. *Journal of Geophysical Research: Atmospheres*, 116(D5).
- Markson, R. (1986). Tropical convection, ionospheric potentials and global circuit variation. *Nature*, *320*(6063), 588-594.
- Markson, R. (2007). The global circuit intensity: Its measurement and variation over the last 50 years. *Bulletin of the American Meteorological Society*, 88(2), 223-242.
- Marshall, T. C., Rust, W. D., Stolzenburg, M., Roeder, W. P., & Krehbiel, P. R. (1999). A study of enhanced fair-weather electric fields occurring soon after sunrise. *Journal of Geophysical Research: Atmospheres*, 104(D20), 24455-24469.

- Nicoll, K. A., Harrison, R. G., Barta, V., Bor, J., Brugge, R., Chillingarian, A., ... & Kubicki, M. (2019). A global atmospheric electricity monitoring network for climate and geophysical research. *Journal of Atmospheric and Solar-Terrestrial Physics*, 184, 18-29.
- Olson, D. E. (1971). The evidence for auroral effects on atmospheric electricity. *pure and applied geophysics*, 84(1), 118-138.
- Peterson, M., W. Deierling, C. Liu, D. Mach, C. Kalb, 2018: A TRMM/GPM assessment of the composition of Generator Current that supplies the Global Electric Circuit, *J. Geophys. Res.*, **122**, 10,025–10,049, doi:10.1002/2016JD026336.
- Reddell, B. D., Benbrook, J. R., Bering, E. A., Cleary, E. N., & Few, A. A. (2004). Seasonal variations of atmospheric electricity measured at Amundsen-Scott South Pole Station. *Journal of Geophysical Research: Space Physics*, 109(A9).
- Reeve, N., & Toumi, R. (1999). Lightning activity as an indicator of climate change. *Quarterly Journal of the Royal Meteorological Society*, *125*(555), 893-903.
- Rodger, C. J., Werner, S., Brundell, J. B., Lay, E. H., Thomson, N. R., Holzworth, R. H., & Dowden, R. L. (2006). Detection efficiency of the VLF World-Wide Lightning Location Network (WWLLN): initial case study.
- Rycroft, M. J., Israelsson, S., & Price, C. (2000). The global atmospheric electric circuit, solar activity and climate change. *Journal of Atmospheric and Solar-Terrestrial Physics*, 62(17-18), 1563-1576.
- Rycroft, M. J., Odzimek, A., Arnold, N. F., Füllekrug, M., Kułak, A., & Neubert, T. (2007). New model simulations of the global atmospheric electric circuit driven by thunderstorms and electrified shower clouds: The roles of lightning and sprites. *Journal of Atmospheric and Solar-Terrestrial Physics*, 69(17-18), 2485-2509.
- Rycroft, M. J., Harrison, R. G., Nicoll, K. A., & Mareev, E. A. (2008). An overview of Earth's global electric circuit and atmospheric conductivity. In *Planetary Atmospheric Electricity* (pp. 83-105). Springer, New York, NY.
- Sátori, G., Williams, E., & Lemperger, I. (2009). Variability of global lightning activity on the ENSO time scale. *Atmospheric Research*, *91*(2-4), 500-507.
- Schmidt, D. S., Schmidt, R. A., & Dent, J. D. (1999). Electrostatic force in blowing snow. *Boundary-Layer Meteorology*, *93*(1), 29-45.
- Siingh, D., Gopalakrishnan, V., Singh, R. P., Kamra, A. K., Singh, S., Pant, V., ... & Singh, A. K. (2007). The atmospheric global electric circuit: an overview. *Atmospheric Research*, 84(2), 91-110.
- Tinsley, B. A. (2000). Influence of solar wind on the global electric circuit, and inferred effects on cloud microphysics, temperature, and dynamics in the troposphere. *Space Science Reviews*, 94(1-2), 231-258.

- Whipple, F. J. W. (1929). On the association of the diurnal variation of electric potential gradient in fine weather with the distribution of thunderstorms over the globe. *Quarterly Journal of the Royal Meteorological Society*, 55(229), 1-18.
- Williams, E. R. (1992). The Schumann resonance: A global tropical thermometer. *Science*, 256(5060), 1184-1187.
- Williams, E. R. (2005). Lightning and climate: A review. Atmospheric Research, 76(1-4), 272-287.
- Williams, E. R. (2009). The global electrical circuit: A review. Atmospheric Research, 91(2-4), 140-152.
- Williams, E., & Mareev, E. (2014). Recent progress on the global electrical circuit. *Atmospheric Research*, 135, 208-227.
- Williams, E., & Stanfill, S. (2002). The physical origin of the land-ocean contrast in lightning activity. *Comptes Rendus Physique*, *3*(10), 1277-1292.
- Wilson, C. T. R. (1909). LVI. On thunderstorm electricity. *The London, Edinburgh, and Dublin Philosophical Magazine and Journal of Science*, *17*(100), 634-641.
- Wilson, C. T. R. (1921). III. Investigations on lightning discharges and on the electric field of thunderstorms. *Philosophical Transactions of the Royal Society of London. Series A, Containing Papers of a Mathematical or Physical Character*, 221(582-593), 73-115.

Figures:

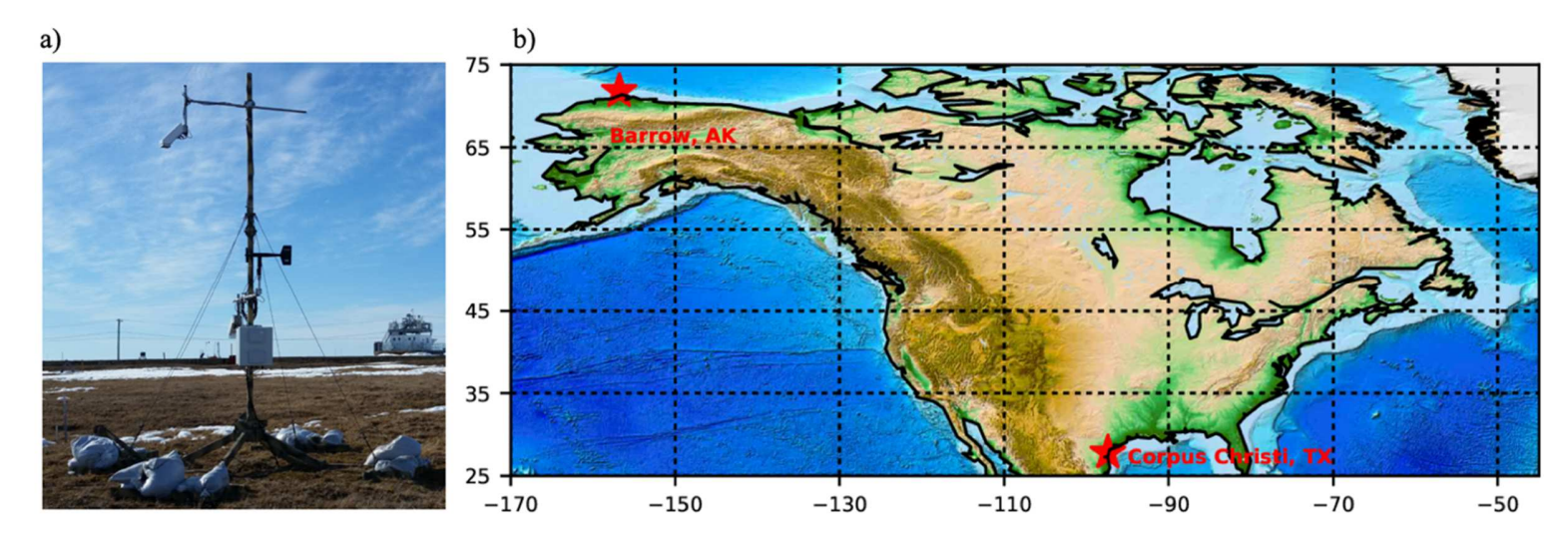


Figure 1: a) the instrumentation setup in Barrow, Alaska, including two CS-110 electric field meters, and one RM-Young Alpine anemometer. b) The geographical locations of the two electric field measurement sites. The distance 6,015 km apart.

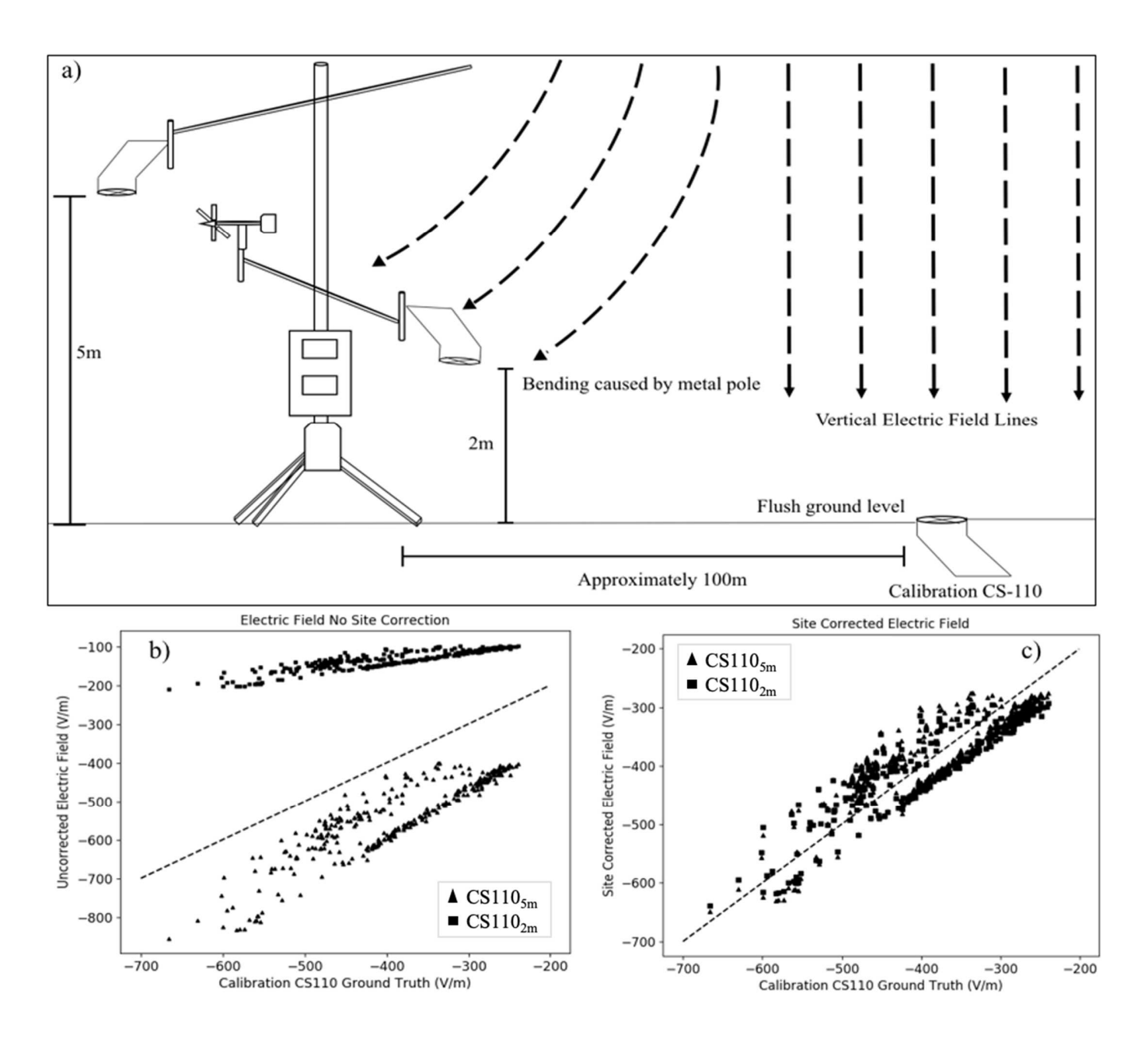


Figure 2: a) Schematic diagram of the vertical electric field calibration process, accounting for the influence of the metal setup and elevation. b) the simultaneous uncalibrated scatter between the $CS110_{5m}$ and $CS110_{2m}$ against the ground truth electric field instrument. c) displays the site corrected scatter of the $2\ CS110$'s versus the simultaneous ground truth. The dashed line shows the perfect one-one correlation. The calibration factor for the CS110-2 is a slope of 0.823 and intercept of 54.9, while the factor for the CS110-3 is a slope of 3.121 and an intercept of 16.69. Calibration took place over the course of approximately a 10-day period from June 13^{th} , 2017 until June 23^{rd} , 2017.

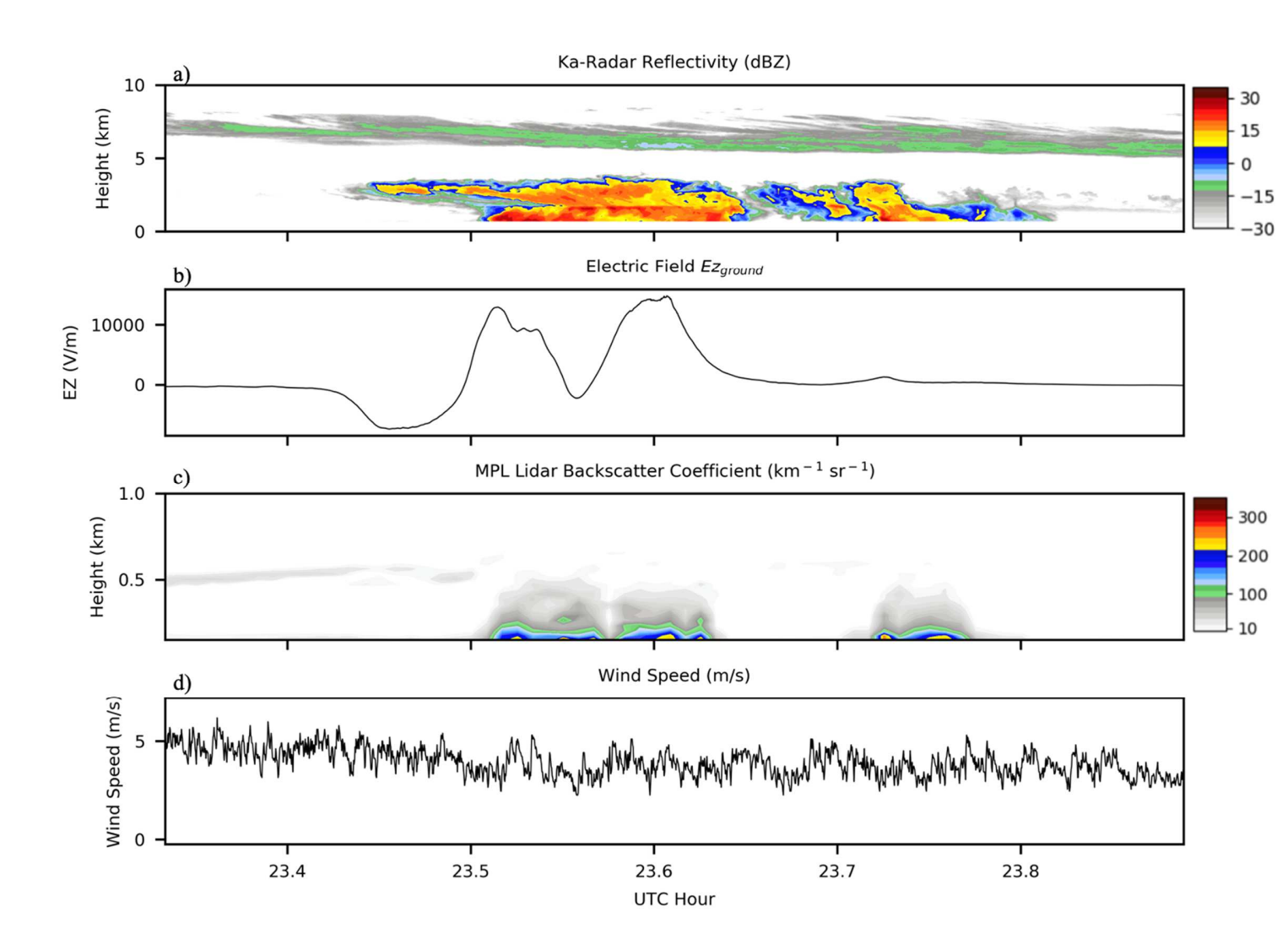


Figure 3: A case of an intense storm electric field event in Barrow, Alaska on July 3, 2017. Panel a) displays the vertically pointing Ka-band radar reflectivity, b) the calibrated vertical electric field measurement at ground surface at a sampling rate of 1 Hz, c) the vertically pointing Micro pulse Lidar backscattering signature (km⁻¹sr⁻¹), and d) the wind speed (m/s) for the day measured at 1 Hz.

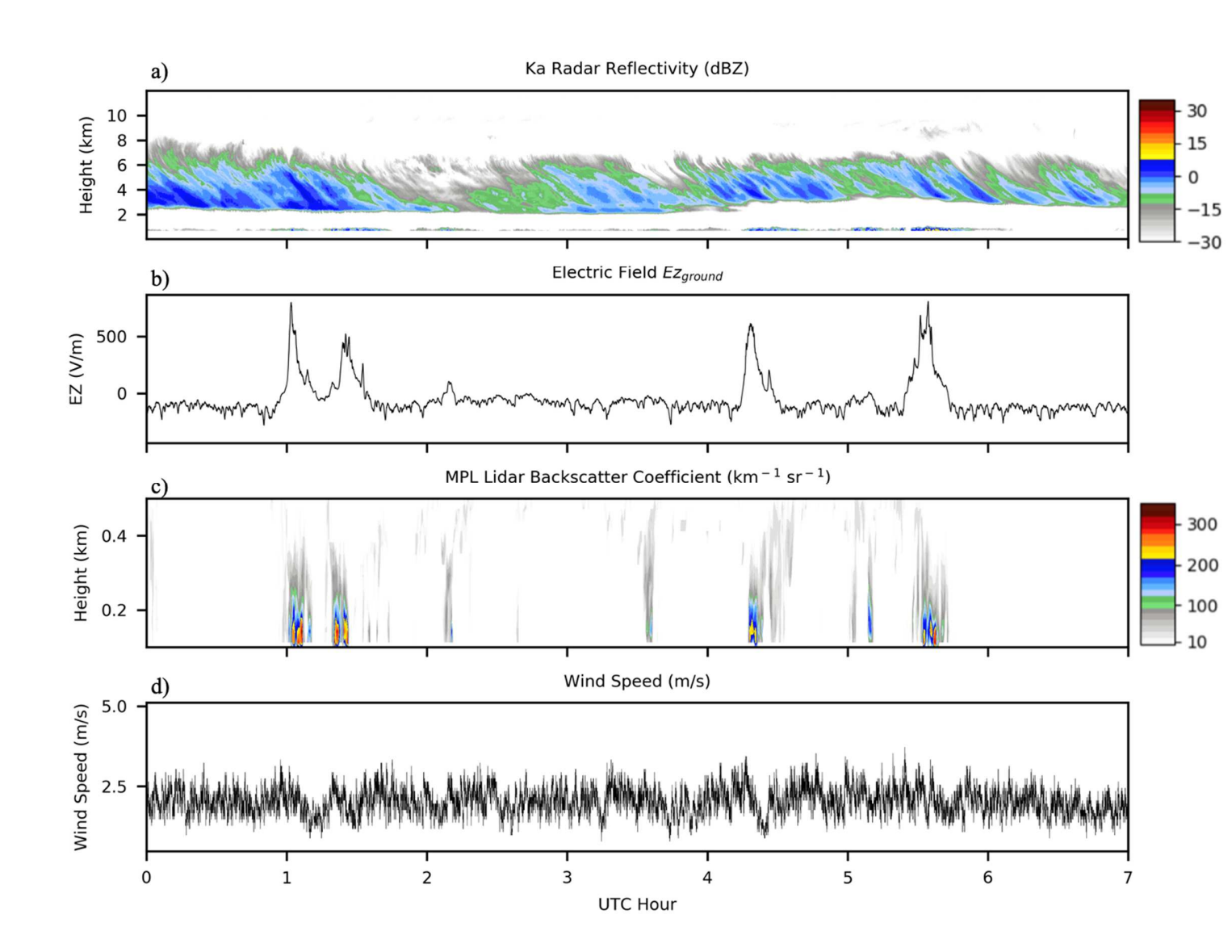


Figure 4: Same as figure 3, except for a Lidar dominated electric field signature case study recorded on August 12, 2017.

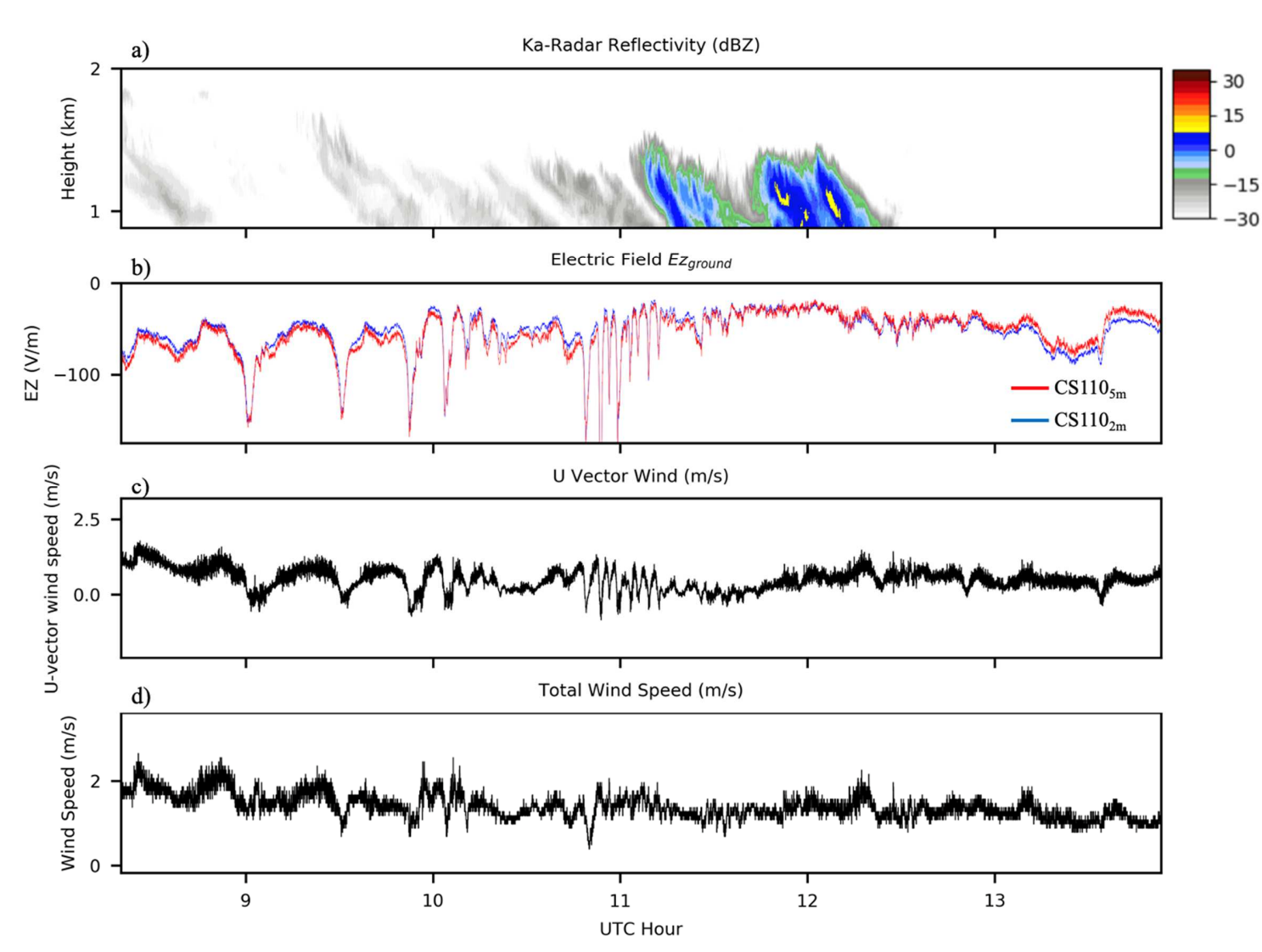


Figure 5: Case study of an electric field event versus wind in Barrow, Alaska on November 9, 2018. Panel a) displays the vertically pointing Ka-band radar reflectivity, b) the vertical electric field measurement at a sampling rate of 1 Hz (red = bottom CS110 and blue = top CS110), c) the U-vector wind speed (m/s), and d) the total wind speed (m/s) for the day measured at 1 Hz.

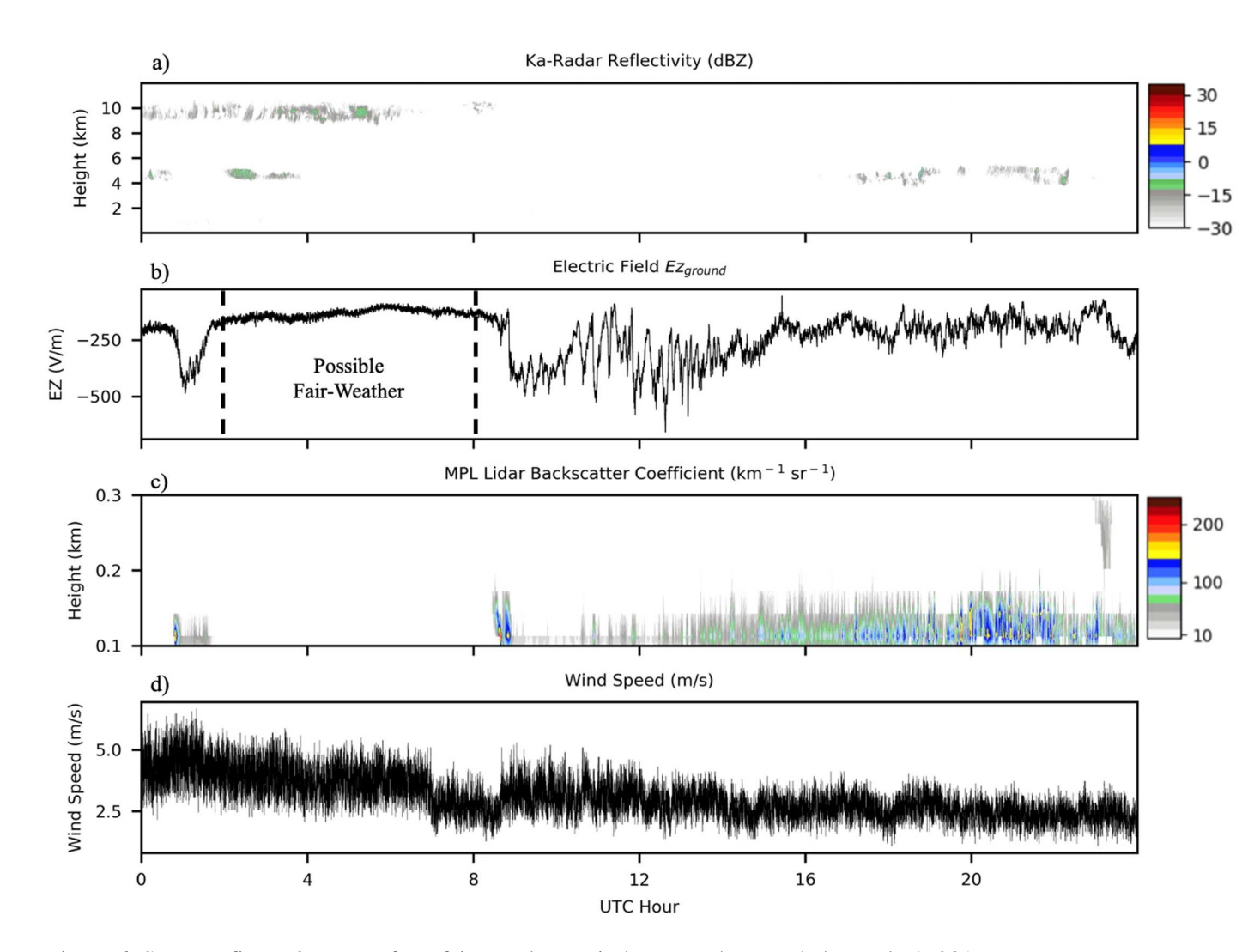


Figure 6: Same as figure 3, except for a fair-weather period case study recorded on July 1, 2017.

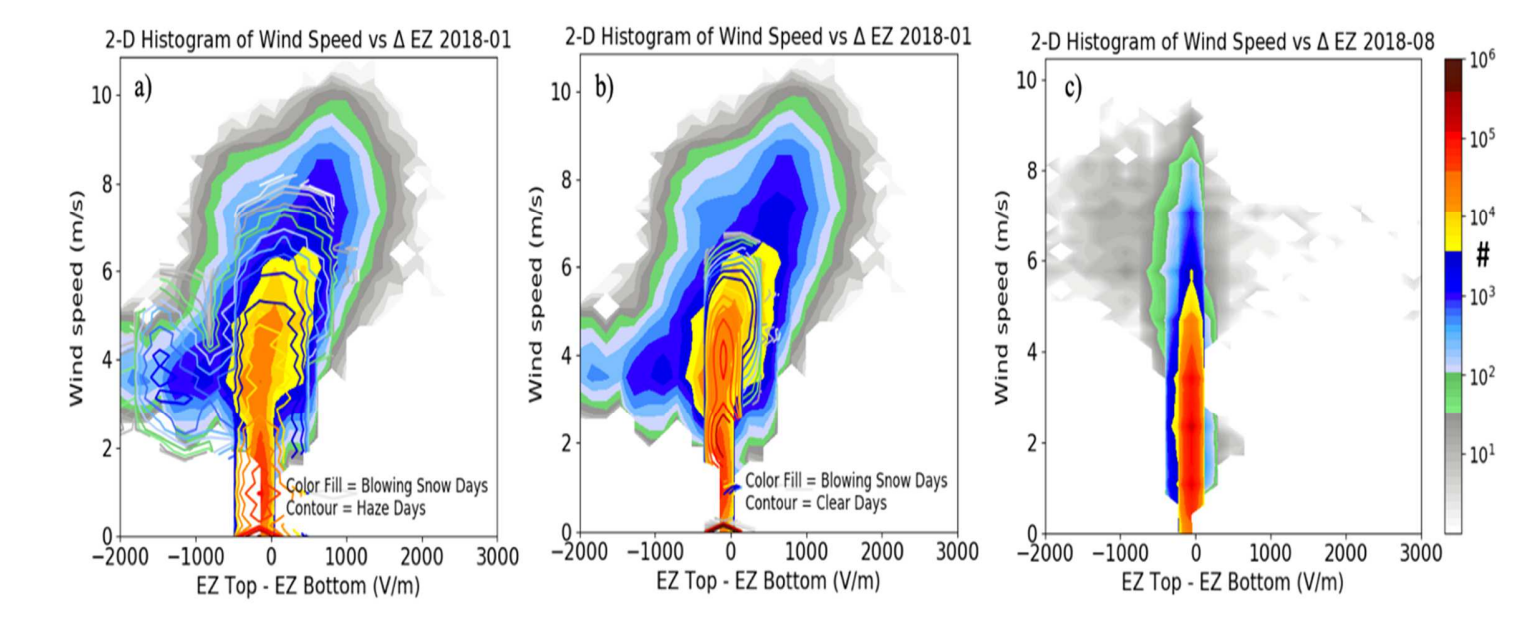


Figure 7: Histogram of the a) difference between the top and bottom CS110 electric field meters versus the wind speed during January blowing snow days (color filled), and January non-blowing snow days with haze (contour). B) Difference between the top and bottom CS110 electric field meters versus the wind speed during January blowing snow days (color filled), and January non-blowing snow days without haze (contour). C) Difference between the top and bottom CS110 electric field meters versus the wind speed during August all sampled data. Blowing snow and haze days were determined using the National Oceanic and Atmospheric Administration (NOAA) Global Surface Summary of the Day (GSSOD) dataset

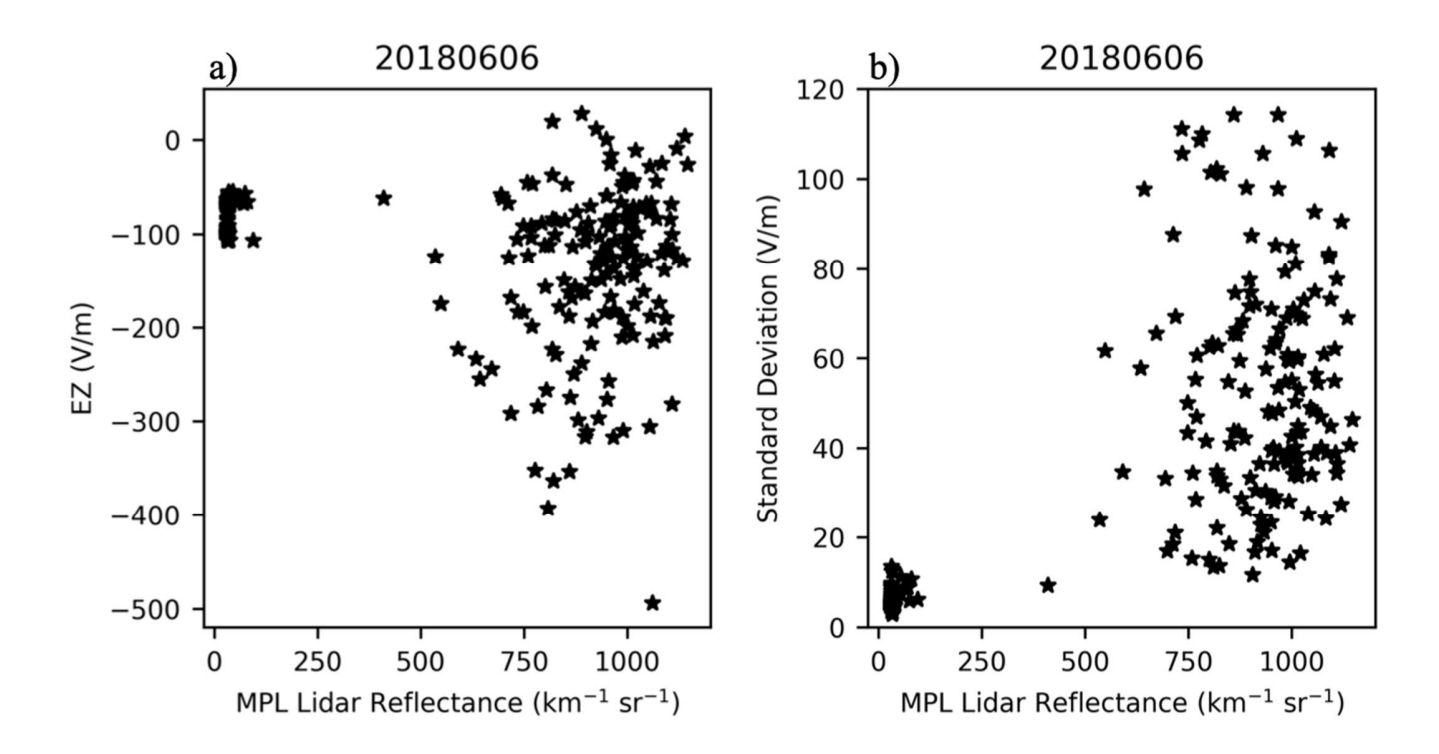


Figure 8: Example scatterplots of 5-minute mean electric-field (V/m) versus the simultaneous 5-minute maximum backscattering (km⁻¹sr⁻¹) overserved by the Micro pulse Lidar (panel a), and the standard deviation of the 5-minute averaged electric-field (V/m) versus the simultaneous 5-minute maximum backscattering (km⁻¹sr⁻¹) observed by the Micro pulse Lidar (panel b).

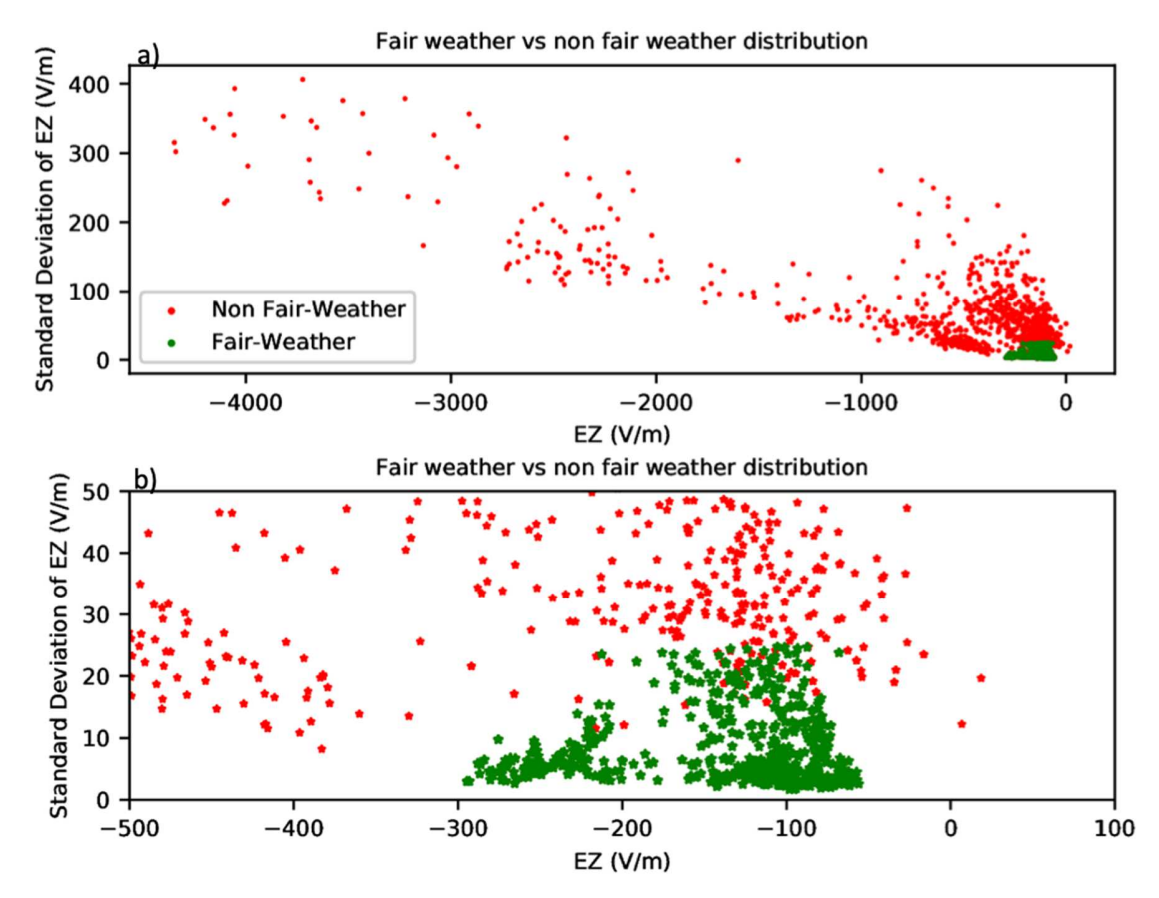


Figure 9: a) Scatter of 5-minute averaged vertical electric field (V/m) measurements versus the 5-minute averaged standard deviation of the electric field (V/m). Green colors represent time periods with a Lidar reflectance of less than 150 km⁻¹sr⁻¹ and red colored stars indicate time periods with a larger Lidar reflectance than 150 km⁻¹sr⁻¹. B) Same as panel a, but zoomed into the fair-weather region. Fair weather time periods were selected to have at least 30 consecutive minutes of less than 25 V/m standard deviation of the vertical electric field. These data were taken in April 9th, April 10th, May 3rd, May 10th, May 30th, August 22nd, September 9th, October 14th, October 15th, and December 18th, all in 2018.

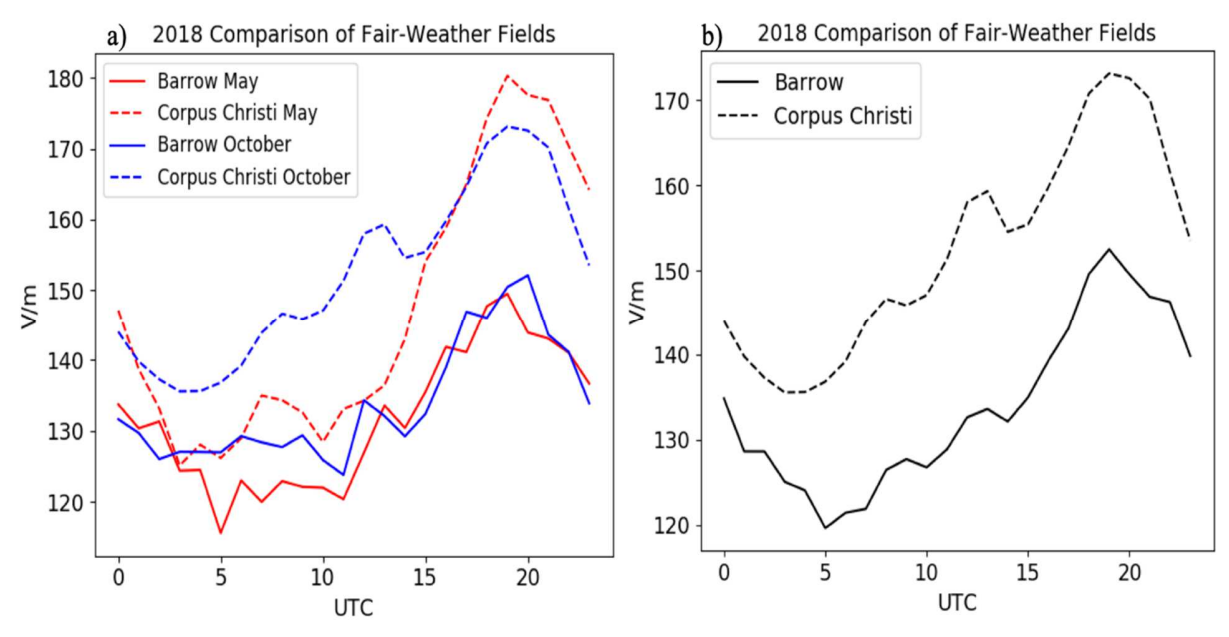


Figure 10: a) Simultaneous diurnal variations of the mathematically selected fair-weather values at Corpus Christi (blue) and Barrow (red) for the months of May (solid) and October (dashed). Panel b) shows the absolute value of the yearly averaged diurnal variation using the mathematically selected fair-weather values at Corpus Christi (blue) and Barrow (red) for 2018.

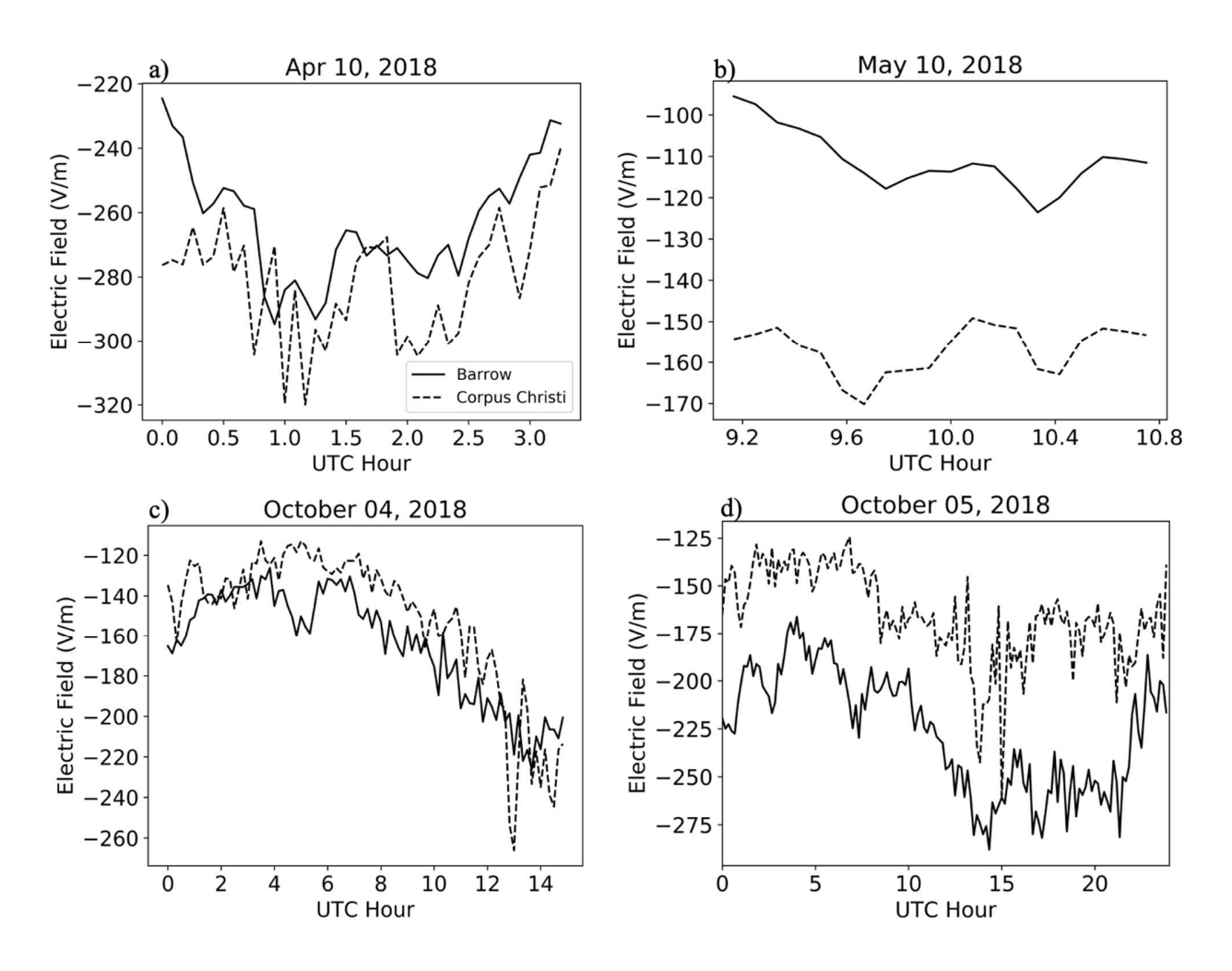


Figure 11: Comparison of simultaneous mathematically selected fair-weather from Corpus Christi (dashed) and Barrow (solid). All panels use a 5-minute averaged electric field. All data from Barrow is displayed using the top instrument (CS110-2).

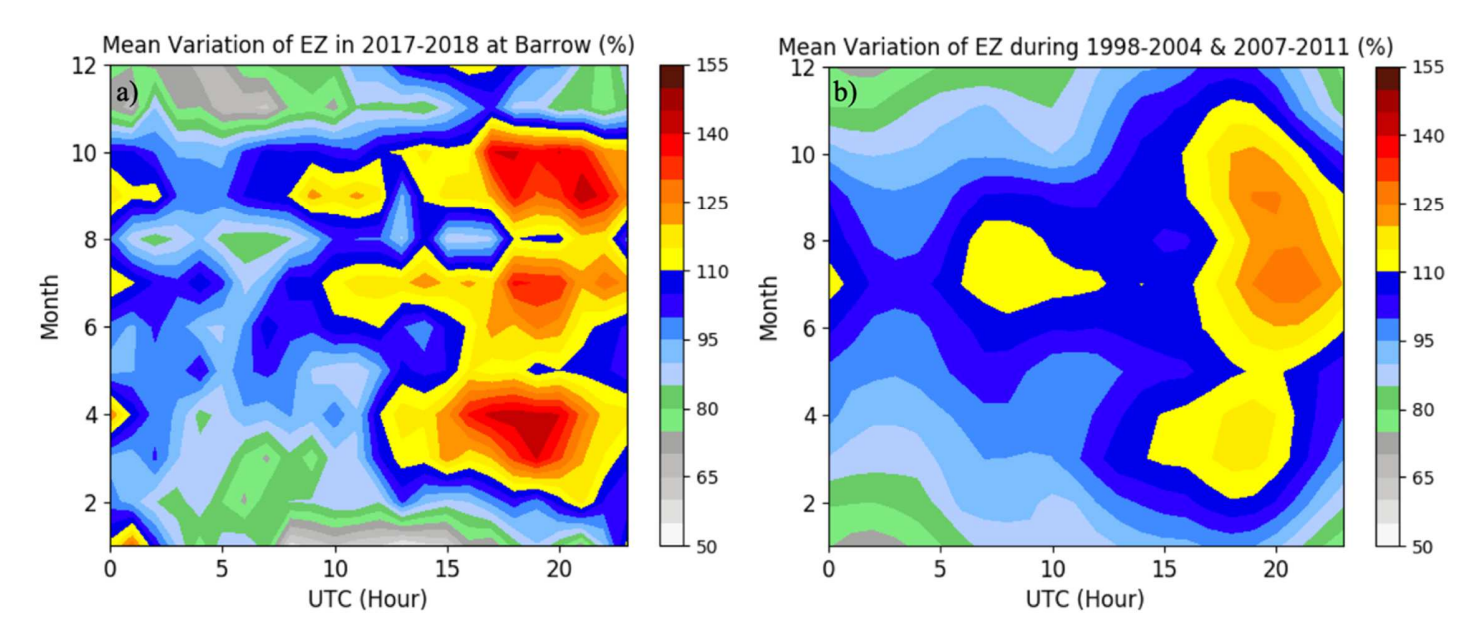


Figure 12: Joint diurnal and seasonal histograms of the mathematically selected fair-weather electric field in a) Barrow and b) Vostok Station Antarctica. All data is collected at a sampling rate of 1 Hz and binned into 1-hourly and 1-monthly bins.